Atmos. Chem. Phys. Discuss., 8, 15941–15996, 2008
www.atmos-chem-phys-discuss.net/8/15941/2008/

Atmospheric Chemistry and Physics Discussions

This discussion paper is/has been under review for the journal *Atmospheric Chemistry and Physics (ACP)*. Please refer to the corresponding final paper in *ACP* if available.

Role of convective transport on tropospheric ozone chemistry revealed by aircraft observations during the wet season of the AMMA campaign

G. Ancellet[1], J. Leclair de Bellevue[1], C. Mari[2], P. Nedelec[2], A. Kukui[1], A. Borbon[3], and P. Perros[3]

[1]Service d'Aéronomie, Université Paris 6, Université Versailles-St-Quentin, CNRS, France
[2]Laboratoire d'Aérologie, Université P. Sabatier-Toulouse, CNRS, France
[3]Lab. Interuniversitaire des Systèmes Atmosphériques, Université Paris 12, CNRS, France

Received: 24 June 2008 – Accepted: 29 July 2008 – Published: 21 August 2008

Correspondence to: G. Ancellet (gerard.ancellet@aero.jussieu.fr)

Published by Copernicus Publications on behalf of the European Geosciences Union.

Abstract

During the wet season of the African Monsoon Multidisciplinary Analyses (AMMA) campaign, airborne measurements of several chemical species were made onboard the French Falcon-20 (FF20) aircraft. The scientific flights were planned in order to document, on one hand the regional distribution of trace gas species related to the oxidizing capacity of the troposphere, and on the other hand their spatial variability in the outflow of mesoscale convective systems (MCSs). The main objectives of this paper are the analysis of the main transport processes responsible for the observed variability, and the discussion of differences and similarities related to the convective transport by 4 different MCSs. This work is needed before using this data set for future studies of the convective transport of chemical species or for modeling work in the frame of the AMMA project. Regarding the regional distribution, five air masses types have been identified using the Lagrangian particle dispersion model FLEXPART, and by considering relationship between the measured trace gas concentrations (O_3, CO, NO_x, H_2O, and hydroperoxides). This paper specifically discusses the advantage of hydroperoxide measurements in order to document the impact of recent or aged convection. The highest values of O_3 are found to be related to transport from the subtropical tropopause region into the mid-troposphere at latitudes as low as 10° N. The lowest ozone values have been always explained by recent uplifting from the monsoon layer where O_3 is photochemically destroyed. Regarding the analysis of the MCS outflow, the CO and H_2O_2 enhancements are related to the age and the southernmost position of the MCS. The analysis of the long range transport of the air masses where convection occurred, shows a connection with the Persian Gulf emissions for the largest CO concentrations in MCS outflow. However for our observations, Lagrangian particle dispersion modelling shows that this possible source is always modified by the convective transport of CO from the African lower troposphere when the air masses encounter a convective system at latitudes below 10° N.

ACPD

8, 15941–15996, 2008

1 Introduction

In order to get a better understanding of the coupling between tranport processes and ozone photochemistry during the West African monsoon period, it is important to build a comprehensive data set including basic meteorological information (e.g. wind and water vapour) and chemical observations. This kind of data set is mandatory for the modelling exercises which will take place during the AMMA framework. Chemical measurements at very low altitudes (<1000 m) already exist in West Africa, e.g. the DECAFE experiment (Cros et al., 1987; Fontan et al., 1992) and the following set up of the IDAF program (IGAC/DEBITS/Africa) which has been initiated in 1994 by French and African scientists within the scope of the DEBITS (Deposition of Biogeochemically Important Trace Species) program (Galy-Lacaux and Modi, 1998). The goals of these projects aimed at studying atmospheric emissions and depositions in the tropical regions and little attention was given to free tropospheric measurements. Measurements at upper altitude were made during the aircraft TROPOZ experiment above the Atlantic ocean but only for the dry season (Jonquieres et al., 1998). The only upper tropospheric measurements available during the wet season are the O_3 and CO data set provided by some on service aircraft operated in the frame of the program MOZAIC (Sauvage et al., 2007). In this paper we present a new data set based on aircraft measurements performed above West Africa, mainly in the mid and upper troposphere, across a large latitude gradient (2° N to 15° N) and near Mesoscale Convective Systems (MCSs). Indeed the scientific flights of the aircraft data discussed here were planned for two different objectives:

- to provide the horizontal variability of trace gas species in the outflow region of MCSs
- to document the regional scale distribution of trace gas species, mainly across the vegetation gradient over Benin and southwestern Niger and through the transition zone between the continent and the Gulf of Guinea.

ACPD
8, 15941–15996, 2008

This new data set is more comprehensive for modelling purposes as it includes other measurements than O_3 and CO, provides a characterization of the mid and upper tropospheric levels and improves the analysis of the impact of tropical convection by comparing 4 flights near MCS. Modelling of the data set is not within the scope of this paper which aims at discussing first the actual meaning of the observations before their use for process studies and model validation. Therefore the goals of this work are the analysis of the main transport processes responsible for the observed variability, and the discussion of differences and similarities related to the convective transport by the 4 different MCSs. Moreover, an additional objective is to look at the complementarity of chemical measurements like O_3, CO, NO_x, H_2O and hydroperoxides for discussing the impact of tropical convection on the chemical composition of the troposphere in Western Africa.

2 Falcon 20 data set

2.1 Flight description

The French Falcon-20 (FF20) aircraft was based in Niamey (13.5° N, 2.1° E) and performed 8 scientific flights from 11 August to 20 August, plus an intercomparison flight with the British BAe-146 aircraft on 16 August (Reeves et al., 2008[1]).

Four flights of the first kind were performed over different MCS and the flight pattern are presented in Sect. 4. Four flights at the regional scale have been conducted during days with low convective activity. For each flight of this second kind, which are discussed in Sect. 3, two long horizontal tracks at 2 or 3 different altitude levels have been performed and the horizontal projection of the flight patterns are shown on the Meteosat (MSG) images in Fig. 1. On 20 August, the goal was to fly along the 1° E line

[1]Reeves, C., Ancellet, G., Borgon, A., F.Cairo, Law, K., Mari, C., Methven, J., Schlager, H., and Thouret, V.: Chemical characterisation of the troposphere over West Africa during the monsoon period as part of AMMA, Atmos. Chem. Phys. Discuss., to be submitted, 2008.

across the core of the African Easterly Jet (AEJ) located at 15° N on this day. During flight of the second kind, meteorological dropsondes have been launched every degrees from the uppermost altitude level of the flight (see Fig. 7a to d in Sect. 3.3). This provides a more detailed picture of the vertical stratification using the water vapour vertical profiles and a mean to check the ECMWF wind data which have been used in the trajectory calculations (Sect. 3.2).

2.2 Instrument description

In this paper, concentrations of O_3, CO, NO_x, H_2O_2, and ROOH will be used together with the standard meteorological measurements provided by the SAFIRE French aircraft management team. Details on the meteorological measurements can be found on the SAFIRE web site (http://www.safire.fr/). The humidity measurements are made by the AERODATA capacitive sensor. The chemical measurements are described in the following sections.

2.2.1 O_3 and CO measurements

The O_3 and CO instrument has been manufactured by Laboratoire d'Aérologie and DT-INSU (CNRS Technical Division). It is a compact instrument developed using the experience gained from the MOZAIC measurement program on commercial Airbus A340 aircraft. The O_3 measurement principle and cells are coming from a commercial fast response ozone analyser (Model 49C TEI Thermo Environment Instruments, USA). The instrument is based on classic UV absorption in two parallel cells (zero, sample), with a precision of 2 ppb, 2% for an integration time of 4 s. It is compensated for aircraft pressure and temperature variations. For O_3, the instrument is calibrated against a NIST referenced O3 calibrator Model49PS, at levels 0, 250, 500 and 750 ppb. No difference (<1%) has been observed during the calibrations before and after the campaign.

The CO analyser is based on a commercial infrared absorption correlation gas analyser (Model 48C, TEI Thermo Environment Instruments, USA). Its accuracy has been

improved by the addition of periodical (20 min) accurate zero measurements, new IR detector with better cooling and temperature regulation, pressure increase and regulation in the absorption cell, increased flow rate to 4 l/min, water vapour trap and ozone filter (Nédélec et al., 2003). The precision achieved for a 30-s integration time (corresponding to the response time of the instrument) is 5 ppb or 5% CO, with a lower detection limit of 10 ppb.

For CO, the instrument has been calibrated before and after the campaign, with no significant difference (<2%). We used a CO in N_2 bottle manufactured by Air Liquide, reference OTO-SL24, 478.8 ppm, NIST referenced ±1%. This bottle was prepared on 14 November 2005, with validity up to 13 November 2008. This bottle has been again measured in 2007 by CNRS and Air Liquide and the concentration was found unchanged. On 23 May 2007, this bottle has been inter compared by DLR with 2 NOAA standards and was found to have a concentration 7.2% lower. No clear explanation is available for these standards differences, all normally comparable to NIST references. CO concentrations given in this paper are not corrected for this difference and must be divided by 1.072 for comparison with the other aircraft.

2.2.2 Peroxide measurements

Peroxide has been measured using modified AEROLASER AL2002 H_2O_2 analyser. Ambient air was continuously drawn by PTFE membrane compressor (KNF N860) through the rear facing inlet and a 2-m Teflon (PFA) tubing into cylindrical 500 cm^{-3} Teflon (PFA) manifold with flow rate of about 10 slm at altitude of 11 km (p=200 torr). The manifold was maintained at the pressure and temperature of the aircraft cabin and served as a sampling volume for several instruments, including the H_2O_2 analyser.

The H_2O_2 measurements are based on the aqueous phase enzyme catalyzed reaction of the peroxides with para-hydroxy phenol acetic acid producing fluorescent dimer (Lazrus et al., 1988). To distinguish between H_2O_2 and organic peroxides (ROOH), both being catalyzed by the peroxidise enzyme, the air sampled from the PFA cylinder at the flow rate of 2 slm is equally divided between two channels. In each channel the

gaseous peroxides are trapped in the liquid solution using 10 turns glass stripped coils. In one of the channels the H_2O_2 is partially destroyed by addition of catalase. The concentration of H_2O_2 in air is derived from the difference of the fluorescence signals from the two channels with accounting for the destruction efficiency of the catalase, about 95% for all measurements as determined by calibration. As the stripping efficiency of the ROOH is different from that of the H_2O_2, the measurements of the organic peroxides mixtures of unknown composition is uncertain. The data presented here as ROOH were derived by taking for all the organic peroxides the same stripping efficiency of 60% as for the methylhydroperoxide (Lazrus et al., 1988). For measurements in remote area or in the free troposphere, the latter is the main organic hydroperoxide and the uncertainty on the ROOH concentration is less important.

The calibration of the instrument has been performed before or after each flight (and occasionally during the flight) using aqueous phase H_2O_2 standard solutions. The standards with mixing ratios (2 to 6)$\times 10^{-7}$ M were freshly prepared by serial dilution of 10^{-2} M stock solution. The concentration of the stock solution has been periodically verified by titration with potassium permanganate.

The base line has been measured about once per hour during the flight by passing the sampled air through the trap containing H_2O_2 scrubber. With freshly prepared solutions the zero signal was about 0.1 V at 5 V full scale adjusted to correspond to about 10 ppb maximum gaseous H_2O_2 concentration. During the same flight the variation of the zero signal was always less than 10% corresponding to H_2O_2 concentration of about 20 ppt.

Based on the stability of the blank the detection limit for the H_2O_2 was estimated to be 50 ppt. The estimated accuracy of H_2O_2 measurements is 20%, including the uncertainties in concentration of aqueous H_2O_2 standards, blanks, gas and solution flow rates, losses of the H_2O_2 in sampling lines and temperature and pressure variations inside the aircraft.

2.2.3 NO_x measurements

The NO_x measurements were performed by the LISA laboratory instrument using two high sensitivity chemiluminescent analyzers (Eco Physics CLD 780 TR). The instrument has been flown during previous field measurements (Marion et al., 2001) and it has been modified for operation on the FF20.

NO is directly measured by the first analyzer. In order to improve the detection limit for NO2 we use a special designed photolytical converter (Eco Physics PLC-762) where NO2 is converted to NO with a high conversion efficiency by the use of a long path photolytic cell (0.91 m) and a 1-kW UV xenon lamp. The Pyrex chamber is cooled to 22°C below the ambient temperature by the use of Peltier elements in order to prevent a possible thermal decomposition of PAN.

The measurement cycles are divided into two different steps. The first step corresponds to the zero determination by introducing excess ozone into a pre-reaction chamber. The second step is the direct measurement by adding ozone into the main chamber. The duration of both steps was 12 s during the campaign, allowing a sample time step of 30 s. For this integration time the detection limit for each NO analyzer is 50 ppt and the precision of the measurements is 0.5%. These values are calculated using a statistical treatment following a French norm (AFNOR NF X20-300).

The NO and NO2 instruments are connected to an air-intake stainless steel with a backward-facing inlet. This design allows us to assume that the air sample corresponds solely to the gas phase and that there is no intake of clouds and aerosols. PFA Teflon is used for all the sampling lines, connectors and valves. The sampling lines are flushed with purified air at ground level in order to prevent contamination, and a subsequent memory effect, of the analytical system. To maintain efficient operation of the analyzers at all altitudes it is necessary to fix the sample flow of each analyzer. Instead of flow rates control with mass flow controllers which can induce a possible modification of the air sample by their metallic surfaces, the flow is controlled by the use of a fixed 200 hPa pressure applied to a critical orifice. The chosen pressure does not allow

ACPD
8, 15941–15996, 2008

operation above 12 km a.s.l. For each analyzer the pressure is controlled with a loop control process using a Teflon needle valve (Whitey) driven by a motor (MKS) and a PID pressure controller (MKS Model 252). Pressure is monitored with a MKS Baratron (Type 122A).

For each flight, calibrations are performed simultaneously for the two chemiluminescent analyzers before take off and after landing. All the procedure is computer driven to ensure the best accuracy of this calibration. A standard 8.47 ppmv NO (Alphagaz) (8 ml/min STP) diluted in a 10 l/min STP N2/O2 synthetic air (Air Liquide) stream allows us to generate 6.77 ppbv NO calibration gas. This gas is then supplied simultaneously to the two analyzers. Since the chemiluminescent analyzers have shown a temperature dependent sensitivity, the calibration coefficients have been corrected.

3 Analysis of the regional vertical cross-section

3.1 O_3, CO, and NO_x variability and air mass attribution

Measured concentrations along the vertical cross-sections at the same longitude (2° E on 13 August 2006 and 19 August 2006 and 1° E on 20 August 2006) are shown in Fig. 2a to d. As expected a significant variability of the chemical species concentrations is observed as a function of altitude and latitude. Hereafter we will discuss the large increase or decrease of the concentrations compared to their mean value. The aim is also to propose an air mass identification using relationship between the measured concentrations which are based on possible transport processes driving their variability. This is the first step needed to assess the meaning of the aircraft data.

3.1.1 Ozone and CO

First, the vertical distributions show large area with high CO values (>140 ppb) and low O_3concentrations (<50 ppb) at altitudes above or near 10 km especially at the beginning of the flight campaign (13 August), the same is true for exactly the opposite case,

ACPD
8, 15941–15996, 2008

i.e. low CO (<110 ppb) and high O_3 concentrations (>70 ppb) mainly in the Northern part of the measurement domain (19 August, 20 August). Only few observations correspond to air masses where CO and O_3 are correlated positively.

In the altitude range 0–4 km, data are obtained mainly from take off and landing of the FF20 in Niamey and Cotonou and significant differences have been observed between the vertical profiles of CO and O_3 at these two places. Ozone concentrations higher than 60 ppb are only observed near Cotonou (6.4° N, 2.5° E) and large CO concentrations are observed at both latitudes but below 2 km above Niamey and up to 4 km near Cotonou. The profiles measured near Cotonou on 19 August 2006 are shown in Fig. 3. Three layers can be identified: the planetary boundary layer up to 1 km with low O_3, a transition layer with the free troposphere up to 2.5 km and the lowermost free troposphere between 2.5 and 3.5 km. Only the transition layer and the lowermost free troposphere show the elevated O_3 and CO values.

Following (Andreae et al., 1994), one can study the chemical history of sampled air masses using the correlation of ozone excess versus CO excess, $\Delta[O_3]$ versus Δ[CO]. Ozone excess is defined here as the ozone concentration corrected by a reference ozone vertical profile which increases linearly with altitude from 20 ppb at 3 km to 50 ppb at 12 km, while CO excess is the CO concentration corrected a mean CO value of 100 ppb corresponding to non polluted tropospheric conditions (Sauvage et al., 2007). In Fig. 4, the correlation plot of $\Delta[O_3]$ versus Δ[CO] shows a negative correlation which suggests a combined influence, on one hand of convective uplifting of low level air masses with high CO and low ozone (i.e. where NO_y was eliminated by wet scavenging in the monsoon layer or where O_3 was titrated in very polluted areas: oil industry, urban cities like Lagos or Cotonou) and on the other hand of dry intrusions from the upper troposphere with high ozone and low CO. Two different lines with high and low gradient have been drawn in Fig. 4 and they correspond to the two main groups identified in this figure. The first one has a gradient of −0.7 close to the value of −1 corresponding to stratospheric intrusion as shown by the analysis of the MOZAIC aircraft data (Brioude et al., 2007), while the higher one (−0.3) can be related to air masses

with ozone chemical loss as measured at midlatitudes in polluted air masses during the winter time (Parrish et al., 1998). Although part of this correlation could be related also to mixing of stratospheric intrusions with polluted air masses, i.e. with large CO values and O_3, this is not very likely at tropical latitudes where the stratospheric intrusions remain at high altitudes and do not cap urban pollution plume as they do at mid-latitudes (Cho et al., 2001). The polluted air mass corresponds to the data collected during landing and take off from Cotonou on 19 August and the corresponding data appears on the plot as the region with positive gradient between $\Delta[O_3]$ and Δ[CO] of the order of 0.3.

3.1.2 NO_x and relative humidity

The NO_x concentrations are only available on 19 August 2006 and 20 August 2006 and ranges between 100 ppt and 400 ppt above 7 km while concentrations ranges from 600–4000 ppt below 4 km. The ratio NO_2 over NO is generally higher than expected suggesting either very reduced NO_2 photodissociation coefficient or high RO_2 radical concentrations considering that $[O_3]$ is often smaller than 50 ppb (not shown). In this paper we will only use the total NO_x concentration to distinguish air masses with high or low NO_x content. The analysis of the NO_x partitioning relevant for O_3 production assessment is not within the scope of this paper. The high NO_x concentrations near 7 km are often related to a relative increase of relative humidity suggesting influence of convective activity (vertical transport of soil emissions or NO production by lightning). Below 4 km, contrary to the CO vertical distribution the highest NO_x concentrations near Cotonou do not reach 4 km but remains below 2.5 km. Therefore transport processes controlling the composition of the transition layer (1–2.5 km) and the lowermost free troposphere (2.5–4 km) are different although homogeneity would have been inferred from the O_3 and CO profiles.

The in-situ relative humidity (RH) measurements made by the Falcon have also been used since it gives information on vertical transport, because high RH can be often related to recent uplift from the Planetary Boundary Layer (PBL) and low RH to subsi-

dence from the upper troposphere. The aircraft RH data have been compared to the dropsonde measurements (see Fig. 7a to d in Sect. 3.3) and are in good agreement.

3.1.3 Air mass clustering using chemical tracer observations

Looking at positive or negative anomalies of the O_3/CO/NO_x/H_2O concentrations along the FF20 tracks, one can identify five different types of air masses:

- Type I where the main characteristics are low O_3 (<50 ppb) and high CO concentrations ($\gtrapprox$150 ppb) i.e. possible export of polluted air mass with O_3 chemical loss in the monsoon layer
- Type II where the main characteristics are opposite to the previous one with low CO ($\lessapprox$100 ppb) and high O_3 concentrations (>70 ppb) together with low relative humidity (RH<30%). This could be related to dry intrusions of ozone rich air masses from the tropopause region into the free troposphere.
- Type III where the main characteristics are low altitudes (<4 km), very high CO ($\gtrapprox$200 ppb) and high NO_x concentrations ($\gtrapprox$1 ppb) while significant O_3 production is also observed with concentrations higher than 60 ppb. These air masses have been encountered near Cotonou.
- Type IV where the main characteristics are [CO]>130 ppb with [O_3]≈70 ppb and [NO_x]≈300 ppt. This group has been chosen as it corresponds to what is expected for an air mass with ozone production related to biomass burning emissions or aged anthropogenic sources (high CO).
- Type V where the main characteristics are 100 ppb<[CO]<130 ppb with [O_3]≈60 ppb, [NO_x]>500 ppt and RH>30%. This group has bee chosen to consider an air mass with ozone production but not clearly related to biomass burning or aged anthropogenic emissions (no elevated CO concentrations).

ACPD
8, 15941–15996, 2008

The Table 1 summarizes the positions of the different air masses types for the 4 flights discussed in this section. Regarding the type III air mass observed near Cotonou on 19 August (Fig. 3), ozone precursors emissions, related to this large city of 1 million inhabitants with frequent air pollution problems, may explain the layer observed between 1 and 3.5 km during the descent to Cotonou. Indeed the comparison between the vertical profiles recorded during landing at 12:00 and take-off 1.5 h later allows the comparison between an air mass 15 km upwind (during take-off) and 10 km downwind (during landing) of the Cotonou emissions. It shows a CO and NO_x increase respectively from 170 pbb to 240 ppb and from 1.5 ppb to 5 ppb, while O_3 increases from 25 ppb to 70 ppb. The latter can be related to the ozone production in the Cotonou plume. Although regional pollution including transport of biomass burning emissions from the Southern Hemisphere can also produce similar level of CO and O_3 production, the southern boundary of this regional pollution plume would have to match exactly the position of Cotonou. This is very unlikely as influence of regional pollution should be found above the ocean. Indeed the influence of this regional pollution is more related to the 170-ppb level of CO recorded upwind during take-off rather than the 240-ppb CO level recorded downwind during landing.

In order to confirm the sources responsible for the chemical characteristics of each group, one must determine the transport processes associated to the different air masses. This will tell us also if the classification based only on correlation between chemical tracers is a valid approach for West Africa.

3.2 Air mass transport analysis

The analysis of the air mass transport was made using the Lagrangian Particle Dispersion Model (LPDM) FLEXPART version 6.2 (Stohl et al., 1998, 2002) driven by 6-hourly ECMWF operational analyses (T106L91) interleaved with operational forecasts every 3 h. The quality of the wind data used for the simulations have been checked using the dropsonde wind data (not shown). The agreement is excellent both for the wind speed and the wind direction, namely the AEJ vertical structure is well reproduced as well as

the southerly flow in the monsoon layer. A southeasterly flow (trade wind layer) is also visible in the 700–600 hPa layer above the Gulf of Guinea on 13 August and 19 August.

FLEXPART includes turbulent diffusion, parameterizations of sub-grid scale convection and of topographic processes, as well as online computation of potential vorticity (PV) for each air parcel. For a given simulation 2000 particles were released during 30 min in a box with a 250-m vertical thickness and a $1^{\circ} \times 1^{\circ}$ horizontal area. This has been done for 23 boxes at different altitudes from 6 to 11.75 km (250 m step) and for different latitudes (every degree) along the vertical cross-section defined by the aircraft flight pattern. Then the positions of the 2000 particles were computed backward in time for 3 days. The 2000 particles mean positions 3 days before the observations are compared to the positions of the observations (released point) in order to produce altitude/latitude plots (Fig. 5a to d) of:

- the relative altitude change of the air mass to identify significant convective ascent or downward transport from the tropopause region
- the relative latitude change of the air mass to identify, on one hand transport from latitudes $<10^{\circ}$ N, i.e. from regions potentially influenced by biogenic emissions from the forest or even by biomass burning emissions from the Southern Hemisphere, and on the other hand from latitudes $>20^{\circ}$ N i.e. from the subtropics where downward transport from the UTLS is often observed
- the relative longitude change of the air mass to assess the fast zonal transport from regions outside of West Africa i.e. mainly corresponding to influence of long range transport from Asia and Middle East.

The discussion of these figures will focus on the transport processes related to the air mass groups which have been identified in Sect. 3.1.3 using the aircraft observations.

3.2.1 Type I air mass

For the 13 August flight (Fig. 5a), the type I air mass at 11.5 km corresponds to a 3–4 km uplift according to the FLEXPART simulation and comes from latitudes always less than 10° N. Upward motion is also resolved by the model for the lower altitude range near 8 km over Cotonou at 6° N with very small horizontal motions. Then vertical transport of pollution sources on the Northern coast of the Guinea gulf (Lagos, oil fields in the Niger delta) is the most likely explanation for the observed large CO values. Indeed MSG images (not shown) indicate deep convective cells at 6° N, 6°–9° E on 10 August 2007 and 11 August 2007. For the 19 August a.m. flight (Fig. 5b), FLEXPART simulations for type I air masses over Gulf of Guinea between 8.5 and 10 km also show local uplift three days before.

3.2.2 Type II air mass

On 19 August, the type II air masses observed North of 11° N in the morning at 10 km correspond to advection from latitudes >20° N. Although no clear subsidence is observed, the strong meridional PV gradient at these latitudes would support the idea of dry intrusion from midlatitudes for type II air masses (Kowol-Santen and Ancellet, 2000). For the afternoon flight (Fig. 5c), type II air masses are again related to advection from latitudes >20° N. The horizontal and vertical extent of the region influenced by this advection between 7 and 10 km corresponds remarkably well to the large section of this flight influenced by the observations labeled as type II air masses. Finally for the 20 August type II air mass at 7.5 km (Fig. 5d), the FLEXPART simulation shows a transport pathway which is different from the type II air mass identified on 19 August with a southeasterly flow linking the observation area with eastern Africa at 10° N, 3 days before. The connection with the UTLS is still possible as there is a downward motion of 500 m per day. It is also noticeable on this day that the vertical stratification of the air mass origin in Fig. 5d corresponds well to three different air mass types in the observations at 5.5 km (type V), 7.5 km (type II) and 12 km (no specific anomalies for

ACPD
8, 15941–15996, 2008

all the parameters, so aged air masses advected by the Tropical Easterly Jet (TEJ)).

3.2.3 Type III air mass

The differences between Niamey and Cotonou have been noticed in Sect. 3.1.1 and are related to differences in the boundary layer dynamics (land/ocean transition for Cotonou and semi-arid region for Niamey), but also to differences in the lowermost free tropospheric dynamics. Indeed near Niamey at the 4-km altitude there is a detrainment layer related to the convergence between the monsoon flow and the Saharan heat low which generally corresponds also to the top of the layer influenced by the AEJ, while near Cotonou the vertical stratification is driven mainly by the southerly flow extending to 3–4 km and the easterly flow above. The latter corresponds to the northern branch of the southeasterly trade winds. This vertical layering frequently observed during the wet season near 6° N along the coast have been discussed by Sauvage et al. (2007).

To study more specifically the origin or the air mass just above the PBL the 19 August near Cotonou, a 4-day backward FLEXPART simulation was performed in two 500-m thick layers at altitudes of 2.25 km and 3.75 km. The 2000 particles are grouped into 5 clusters, the position of which are shown as a function of time for the two layers (Fig. 6). Advection was quite slow in both layers with a weak southwesterly flow and the impact of the trade winds appears only 4-days before at 3.75 km. The long residence time of the air mass above the coast line near Cotonou means that the air mass influenced by biomass burning from the Southern Hemisphere is probably dominated by mesoscale circulations near the coast. Similar effect have been documented at mid-latitudes for pollution transport in large cities located near the sea (Zhang et al., 1998; Drobinski et al., 2007). Hypothesis of a significant influence of local emissions in the ozone production observed near Cotonou is then supported by this weak influence of the regional transport.

ACPD
8, 15941–15996, 2008

3.2.4 Type IV air mass

On 19 August the type IV air masses at low latitudes between 2 and 4° N near 7.5 km correspond to air masses coming from the Southern Hemisphere (10° S, 20° E). Therefore ozone precursors observed in this air mass can be related to the active biomass burning which is very common during the austral winter (Mari et al., 2008). This is also consistent with the high CO/NO_x ratio (200) compared to the weaker ratio (20) observed in type V air mass. The first evidences of southern hemispheric fire intrusions were described by Sauvage et al. (2005) based on the MOZAIC profiles over Africa. These authors showed that elevated concentrations of ozone observed between 600 and 700 mb over West Africa during the the wet season originated from fires in the Southern Hemisphere. In the framework of the AMMA campaign, regular ozonesoundings were performed at Cotonou, which is located near the Gulf of Guinea and therefore can be influenced by the pollution from the southern hemispheric fires. In Mari et al. (2008), one can note that the ozone peak on 17 August Cotonou ozonesounding profile corresponds to the active phase of the African Easterly Jet – South (AEJ-S) when the Gulf of Guinea is under the influence of the fire plumes. Actually, the F-F20 flights period is included in this second active phase of the AEJ-S which goes from 9 August to 31 August.

3.2.5 Type V air mass

The air mass trajectory analysis is very interesting for the type V air mass as it is the group where the identification of the sources is the most uncertain. For air mass identified between 4° N and 6° N near 7.5 km on 19 August in the morning, the FLEXPART simulation shows a slow horizontal transport. Upward motion is not clearly resolved by FLEXPART for the air mass at 7 km but is shown for air masses arriving 1.5 km higher and originating from Northern Nigeria. Notice that the RH vertical stratification revealed by the two dropsondes in this area shows that the 7.5 km level is at the lower boundary of a very humid layer between 7.5 and 10 km (see Fig. 7a to Fig. 7d in next section).

ACPD
8, 15941–15996, 2008

So the O_3 production in this type V air mass could be explained by an upward transport of ozone precursors, namely organic compounds from biogenic emissions and by the high NO_x concentrations related to either lightning and/or NO_x soil emission. During the afternoon flight, the 3-km uplift of air masses located initially from Northern Nigeria is in good agreement with the type V air mass observed between 8° N and 11° N at 7.5 km. This area correspond also to the 4 dropsondes where high RH is observed at many vertical levels between ground and the aircraft (see Fig. 7a to d in next section). Looking at the comparison of the trajectories for the two type V air masses of the am and p.m. flights, it is encouraging to see that they are similar while the two air masses were identified using only chemical tracer data. This demonstrates that the classification of Table 1 which is based on relative impact of different transport processes is indeed in good agreement with a direct meteorological analysis.

For the type V air mass at 6 km from 11° N to 13° N on 20 August (Fig. 5d), it shows a slow zonal advection and a 1–2 km downward motion over West Africa (air mass at 12° E 3 days before). Although no indication of upward transport is shown by the FLEXPART simulation, the slow zonal motion increases the probability for encountering convection with uplifting of an air mass. The low CO necessary for this group is explained by the fact that, if convection has occurred, it must have developed over an area with moderate vegetation and little influence from biomass burning emissions. The high NO_x concentrations and subsequent O_3 production characteristic of the type V air mass must be related to lightning and/or upward transport of soil emissions at latitudes above 10° N.

3.3 Variability of the hydroperoxides measurements

The H_2O_2 concentrations are shown in Fig. 7a to d together with the relative humidity and the fraction of H_2O_2 relative to the total concentration of hydroperoxides. The latter parameter is quite useful in the mid and upper troposphere because, for air masses showing a clear decrease of H_2O_2 concentrations, it helps to distinguish on one hand the impact of mixing by upper tropospheric air where there is low ROOH and on the

other hand fast convective upward transport of depleted H_2O_2 air masses within the monsoon layer where ROOH will decrease more slowly than H_2O_2 in presence of wet scavenging and aqueous chemistry (Snow et al., 2007). For elevated H_2O_2 concentrations, the H_2O_2 fraction can measure the atmospheric chemical processing of an air mass which is proportional to the duration of the atmospheric oxidation processes responsible for OH formation. This will decrease the H_2O_2 fraction as the hydrocarbon oxidation will produce ROOH (Heikes et al., 1996).

Regarding the H_2O_2 vertical distribution, there is a negative vertical gradient in the free troposphere with a maximum near 2 km (1.5–1.8 ppb) and lowest values ranging from 200 to 500 ppt near 10 km. Below 2 km, H_2O_2 concentrations decreases with a significant sink related to wet scavenging and surface removal. Looking more precisely at the free tropospheric data, the H_2O_2 concentrations shows a sharp drop near 7 km with concentrations often being above 1 ppb below 7 km and decreasing below 600 ppt above 8 km. This is in good agreement with previous observations over the ocean (Heikes et al., 1996; Snow et al., 2007) showing that it is the direct result of a large production of HO_x and RO_2 at altitudes near 2–4 km.

Following (Heikes et al., 1996), a positive correlation is expected between $[H_2O_2]$ and $[O_3]^*[H_2O]/[CO]$ since OH will be proportional to the ratio $[O_3]^*[H_2O]/[CO]$. Since the photochemical time scale for H_2O_2 is short enough (1–2 days), this correlation will hold as long as recent vertical transport and related wet scavenging in the PBL cannot compete with the net photochemical equilibrium. In Fig. 8, the correlation plot shows that the positive correlation is kept although it is less compact as the ratio $[O_3]^*[H_2O]/[CO]$ increases. Indeed air masses related to a recent vertical transport corresponds to a small fraction of the observed data (mainly type I air mass) and it cannot control the correlation plot. It was different for the correlation between CO and O_3 because they have longer photochemical time scale in free troposphere and a larger fraction of the data collected in West Africa during the wet season may have been influenced by upward transport on a time scale of 1–2 weeks. The decrease in the compactness of the plot are for the highest values of $[H_2O]$ in the troposphere (3–6 km) where the age

of the air mass are largest and the range of H_2O_2 concentrations depends on the air mass composition following air mass transport. For example an increase of NO_x and a decrease of soluble carbonyl compounds will reduce the H_2O_2 formation. This dependence of hydroperoxide data with the influence of convective transport makes the use of these data very useful to continue the discussion about the link between the air mass types identified in Sect. 3.1.3 and the dynamical processes.

3.3.1 Type I air mass

Considering type I air mass, this study shows that low H_2O_2 concentrations (<500 ppt) are related to these air masses, this is consistent with the efficient wet scavenging and/or reaction of H_2O_2 with SO_2 related to recent uplifting by well developed MCS. The H_2O_2 fraction is of the order of 0.4 lower than the fraction for other air masses with similar H_2O_2concentrations (H_2O_2 fraction near 0.8). Indeed this corresponds to the lower solubility of ROOH which is less depleted than H_2O_2 during convective uplifting.

3.3.2 Type II air mass

For the type II air mass observed in the upper troposphere, H_2O_2 is as low as the concentrations observed for type I air mass. This can be explained by the low water vapour concentrations which cannot maintain elevated HO_x radical and H_2O_2 production. Regarding the H_2O_2 fraction, the values are larger than for type I air masses This is in good agreement with the fact that type II air masses could correspond to advection of upper tropospheric air from the subtropics. Indeed in this case mixing with upper tropospheric air dominates the other sinks of hydroperoxides.

3.3.3 Type IV air mass

In previous papers (Lee et al., 1997; Snow et al., 2007), the possibility of hydroperoxide formation in biomass burning plumes have been shown, especially for H_2O_2. This is not observed in our study where concentrations of H_2O_2 remain near 700–800 ppt

ACPD
8, 15941–15996, 2008

at 7.5 km. It is explained by the fact that the time scale for the transport of Southern Hemisphere biomass burning near the coast of West Africa is longer than 1–2 days. Indeed in this case, the H_2O_2 produced within the plume does not contribute anymore to the hydroperoxide budget. The H_2O_2 fraction is below 0.7 so consistent with moderate atmospheric processing being able to increase the formation of ROOH. So the time scale for the transport of biomass burning cannot exceed 3–4 days.

3.3.4 Type V air mass

The horizontal variability of H_2O_2 near 7.5 km shows that the higher values (>1 ppb) are often observed in the type V air mass where high NO_x and RH>50% are present. This indicates that upward transport plays a significant role in type V air mass. Indeed uplift of humid air mass from the lower troposphere increases the HO_x radical production necessary for subsequent hydroperoxide formation. Since we expect H_2O_2 removal in the humid PBL, this implies that the observations correspond to convective processes older than at least 1–2 days, i.e. the time scale for hydroperoxide chemical production. It is often the case for the flights discussed in this section since they have been performed in clear air far away from convective systems. Considering that the lifetime of NO_x is longer in the free troposphere than the hydroperoxide lifetime, this hypothesis is also in good agreement with the elevated NO_x concentrations resulting from either lightning processes in the convective system or upward transport of soil emissions which are maximum over wet continental surfaces (Delon et al., 2008; Stewart et al., 2008). It is also interesting to examine the H_2O_2 fraction for the type V air mass where there is this relative H_2O_2 enhancement. We can notice high fractions (>75%) on 19 August while the fraction drops to 50% on 20 August. This means that atmospheric chemical processing during the upward transport has been more intense for the 20 August type V air mass compared to the 19 August type V air mass. This is also consistent with lower RH and NO_x values on 20 August. Indeed a longer time since exposure to surface emissions and uplifting, allows on one hand dehydration of the air mass in the upper troposphere before subsidence to lower altitudes near 8 km

and on the other hand NO_x chemical conversion. One can notice also that the trajectory analysis also shows more evidence of nearby upward motions for the 19 August type V air masses.

4 Comparison of the MCS flight

4.1 Chemical composition of the MCS outflow

Four Mesoscale Convective Systems (MCS) have been studied using the FF20 aircraft: 3 over the Sahelian region (11 August, 14 August, 17 August) and 1 over the Benin forest (15 August). The FF20 tracks are superimposed on the images of the MCS brightness temperatures at the times when the FF20 starts the MCS upper altitude exploration (Figs. 9 to 12). The measurements always start at the western bound of the M shape flight track and the aircraft stays at the the same altitude (12 km) during the 2.3 h upper altitude exploration. So during the flight, the MCS moves westward by approximately 1.5° from its initial position shown in Figs. 9 to 12.

4.1.1 MCS characteristics

On 11 August, the upward development revealed by MSG images indicates a strong MCS which has formed 2 days before over the border between Nigeria and Tchad (10° N, 15° E) and was followed by a second one which has dissipated east of Niamey. The aircraft has flown mainly in the outflow region of the first MCS after its transport northward to Western Niger. On 14 August, another strong MCS has been studied East of Niamey with the beginning of the flight being near the leading edge of the MCS and the end in the convective area. The MCS is significantly younger compared to the previous one as it started only 15 h before the FF20 flight, over the Zinder region (14° N, 10° E) before moving westward at the same latitude. On 15 August, the MCS is located at latitudes farther south (10° N) over Benin and it is significantly smaller

than the previous ones. It corresponds to the southern tip of a decaying system which formed over Tchad (15° N, 17° E) 36 h before. Again the beginning of the flight took place in front of the MCS and the end in the outflow. Finally on 17 August, the MCS is also rather weak during the measurement period over Niamey. It actually dissipated during the FF20 flight with the beginning of the flight in the leading edge of MCS and the end in the convective area. This system has formed over the Aïr region (18° N, 6° E) 18 h before the Falcon flight and has moved southward to Niamey. Let us examine the horizontal variability of the measured chemical species in the outflow of these MCS.

4.1.2 Ozone and CO variability

Three flights (15 August, 14 August, 11 August) show large sections of the flight with CO concentrations higher than 140 ppb and up to 190 ppb on 15 August. The question arises whether it is related to transport of CO surface emissions uplifted from the West African PBL or whether the elevated CO is already present in the upper altitude air mass because of long range transport from regions outside the AMMA region. On 17 August, the encountered CO concentrations are lower than for the other as they never exceed 140 ppb. On 15 August and 17 August, the areas with the highest CO values are found behind the convective system in its outflow rather than in its leading edge. This points toward a significant role of the convective transport rather than regional scale circulation on the large concentrations encountered. It is less obvious for the 14 August where the high CO concentrations are located in the northern part of the measurement area, which is less influenced by the MCS outflow.

Ozone concentrations are rather weak (<50 ppb) for all the MCS flight except on 15 August when they exceed 50 ppb mainly in the northern part of the convective area.

4.1.3 Hydroperoxide variability

The H_2O_2 distributions show areas of high concentrations (>600 ppt) but their horizontal extent are always smaller than the high CO patterns. Looking at the average

ACPD
8, 15941–15996, 2008

concentrations over the whole convective area, the concentrations are smaller (300–400 ppt) for the most active MCS on 11 August and 14 August. This is consistent with the hydroperoxide sink in the humid PBL before rapid upward transport at upper altitudes by the convective system. This hypothesis is also supported by the low values of the H_2O_2 fraction (<50%) also observed for these two flights since one expect ROOH to be less depleted in the humid PBL. The only small area with large H_2O_2 during the 11 August is found in the southwestern corner with also low H_2O_2 fraction and moderate CO concentrations of the order of 120 ppb. This would indicate that this particular part of the MCS convective area has been influenced by a significant amount of atmospheric processing to increase ROOH. It is not so surprising that old masses are interleaved with fresh convective outflow in the older MCS.

The H_2O_2 concentrations are in the range of 500–600 ppt for the less active MCS on 15 August and 17 August. The H_2O_2 fraction remains high for the layer with the largest H_2O_2 concentrations (>600 ppt) on these two days. This would be consistent with an upward transport from the humid PBL which took place 1 or 2 days before the measurement to allow some H_2O_2 production with significant ROOH increase compared to H_2O_2.

To summarize the analysis of the CO, O_3 and H_2O_2 concentrations shows that convective transport drives the variability of the chemical composition when they are intercompared. The main key parameters appear to be the lifetime and the latitudinal position of the MCS during its evolution. Indeed one first notices no influence of polluted air mass on 17 August due to the northern origin of the MCS. Second regarding the 11 August and 15 August MCS, transport from the lower layers at latitudes around 10° N may explain the area with large CO concentrations. The latter conclusion is based on the observation of a negative latitudinal CO gradient by other aircraft in the lower layers (Reeves et al., 2008[1]). Third the lifetime of the MCS allows for more H_2O_2 production and consequently also on available HO_x radicals. To support this interpretation of the observed comparison of the 4 MCS, it is also necessary to conduct an analysis of the air mass transport using the meteorological analysis. For example, this would help to

ACPD
8, 15941–15996, 2008

understand why there are large CO concentrations on 14 August while the MCS has remained above 13° N during its lifetime or why there is larger O_3 concentrations for the 15 August MCS compared to the 11 August MCS.

4.2 Air mass transport analysis

The analysis of the air mass transport was made using again FLEXPART version 6.2 driven by 6-hourly ECMWF analyses (T106L91). For a given simulation 1500 particles were released during 60 min in a box with a 1-km vertical thickness and a 1°×1° horizontal area. This has been done for approximately 17 boxes at the same altitude (the altitude of the MCS survey flight) and for different latitudes and longitudes (every degree) along the aircraft track. Owing to the limited area of the MCS survey and the limited horizontal resolution of the ECMWF analysis, the variability of the trajectories for a given flight is rather small and is not really suitable for a detailed analysis of mesoscale structure in the chemical composition. However the comparison of the trajectories from one MCS to the other one is possible. So we have focused our attention on a single trajectory computed from a single position in the outflow of the MCS.

First the 4 FLEXPART trajectories ending at the observed MCS altitude can be compared (Fig. 14). It is interesting to observe that a significant fraction of particles have been uplifted by more than 5 km in the FLEXPART simulations for the 3 days with high CO values observed in the outflow of the MCS. FLEXPART is then able to reproduce some convective transport in this region. Part of this transport is already resolved in the ECMWF analysis itself since it remains when the FLEXPART convection is switched off. The cluster in the lower layers indicate a source region located above the Arabic Peninsula 5 days before and with a likely connection further ahead with the Persian Gulf. Notice that this connection is not present on 17 August when CO remains low around the MCS. The question arise about the influence of the significant emissions related to the oil industry in this region. This transport pathway is different from the one analysed in (Barret et al., 2008), where MLS UTLS CO observations preliminary adjusted towards a climatological tropical profile have been assimilated. At and above

ACPD
8, 15941–15996, 2008

150 hPa the main contributors are westward transport by the Tropical Easterly Jet and the Asian Monsoon Anticyclone of Asian polluted air masses that have been uplifted up to 100 hPa resulting in maxima CO concentrations over North Africa around 25° N. Even if FLEXPART is able to resolve some uplifting, it may miss strong upward transport due to MCSs encountered along the trajectories. To account for this contribution to the CO distribution, occurrence of observed MCS by MSG was searched along the FLEXPART trajectories. Examples of the cluster positions are shown on the top of MSG images at 00:00 UT on the measurement day and 00:00 UT on the previous day in Fig. 13. This analysis has shown that for the 11 August and 14 August MCS, another MCS encountered previously must have changed the chemical composition of the advected air mass, while for the 15 August and 17 August MCS it is the influence of the MCS sampled by the aircraft which must be taken into account. Therefore assuming that the MCS occurrence connect efficiently the lower troposphere below 2 km and the upper troposphere above 10 km, we calculated a backward flexpart simulation releasing 1500 particles at the base of the MCS, i.e. in a 1°×1° box between 1.5 and 2 km, at the time when the upper altitude trajectory encounters the MCS. This low level backward simulation was performed on the MCS encountered respectively on 10 August at 10° N, 15° E and on 13 August 10° N, 20° E for the 11 August and 14 August cases, while it was performed for the sampled MCS at 00:00 UT on the measurement day for the 15 August and 17 August cases. Looking at Fig. 15, it shows that a significant fraction of the 1500 particles are coming from the equatorial region below 6° N for the 3 MCS corresponding to the elevated CO observed by the aircraft in the upper troposphere. More precisely, the fractions of particles south of the 6° N limit are respectively 10%, 19% and 34% for the 11 August, 14 August and 15 August observations. The numbers are even higher (55%, 50% and 35%) if we choose the 10° N limit which often corresponds to the largest CO meridional gradient. This implies that the biomass burning source in the Southern Hemisphere contributes to the CO distribution in the Northern Hemisphere upper troposphere as far as 15° N. This is in agreement with (Barret et al., 2008) who showed that below 150 hPa, convective uplift

ACPD
8, 15941–15996, 2008

of air masses impacted by biomass burning in Southern Africa within the West African Monsoon region between 0° N and 12° N is the main contributor to the latitudinal CO maximum. The fact that the largest O_3 concentrations are found for the 15 August MCS indicates also that this pathway is probably the dominant one. Indeed the 15 August case corresponds to the largest fraction of particles south of 6° N, while it is not very different from the other MCS looking at the middle east pathway revealed by the upper level trajectories (Fig. 14).

5 Conclusions

The analysis of the O_3, CO, NO_x, H_2O and hydroperoxide data of the FF20 was done at two different spatial scales: regional variability along a North/South cross section from the Guinea Gulf to the Sahara desert and characterization of the outflow of 4 different MCSs. By considering extrema values of the 5 chemical species measured at several altitudes in the troposphere, 5 different air mass types have been identified. The dynamical characteristics assumed from relationships between the chemical data have been supported by a study of the air mass transport using Lagrangian Particle Diperision Modelling with FLEXPART. It has been shown that the air mass type 2 corresponding to the largest O_3 values is related to the transport of ozone from the subtropical tropopause region at altitudes between 5 and 10 km and down to 10° N. The opposite case is the type 1 air mass corresponding to the lowest O_3 values which were shown to be related to recent uplifting from the monsoon layer where O_3 is photochemically destroyed. The 3 other air masses are characterized by some O_3 production related to (i) urban pollution near Cotonou (ii) biomass burning from the Southern Hemisphere (iii) chemical evolution during 1–2 days following convective transport (high NO_x, high H_2O_2 air masses). Some of the previous features are already noticeable in O_3 and CO correlation plots and also in the correlation of H_2O_2 with a OH concentration proxy ($[O_3]$*$[H_2O]/[CO]$). Regarding the analysis of the observations in the outflow of different MCSs, it was shown here that the increase of CO and H_2O_2 and the associated

ACPD
8, 15941–15996, 2008

chemical reactivity necessary for subsequent O_3 formation, are directly related to the position and the lifetime of the MCS during its evolution. Increased lifetime (>1.5 days) allows more H_2O_2 formation, while a trajectory of the MCS crossing the 10° N latitude increases the probability of CO transport to the upper troposphere. The analysis of the long range transport of the air masses where convection occurred, mainly shows a connection with the Persian Gulf emissions for the largest CO concentrations. For our observations this possible source is always modified by the convective transport of CO when the air mass encounters a convective sytem at latitudes below 10° N. Indeed combining FLEXPART analysis of the low level transport with MSG MCS observations has shown that the northward transport of biomass burning from the Southern Hemisphere followed by convective transport in the latitude band 5°–10° N probably dominates the chemical composition in the upper layer when large CO concentrations are encountered.

Acknowledgements. Based on a French initiative, AMMA was built by an international scientific group and is currently funded by a large number of agencies, especially from France, the UK, the US and Africa. The UMS SAFIRE is acknowleged for supporting the FF20 aircraft deployment and for providing the aircraft meteorological data (humidity and dropsondes). This work was supported by the AMMA EC project and INSU. Franck Roux (Laboratoire d'Aérologie) is acknowledged for work on flight planning and validation of the dropsonde data and Ariane Bazureau (Service Aéronomie) is acknowledged for work on FLEXPART modelling.

References

Andreae, M. O., Anderson, B. E., Blake, D. R., Bradshaw, J. D., Collins, J. E., Gregory, G. L., Sachse, G. W., and Shipham, M. C.: Influence of plumes from biomass burning on atmospheric chemistry over the equatorial and tropical South Atlantic during CITE3, J. Geophys. Res., 99, 12 793–12 808, 1994. 15950

Barret, B., Ricaud, P., Mari, C., Attié, J. L., Bousserez, N., Josse, B., Le Flochmoën, E., Livesey, N. J., Massart, S., Peuch, V. P., Piacentini, A., Sauvage, B., Thouret, V., and Cammas, J. P.: Transport pathways of CO in the African upper troposphere during the monsoon season:

a study based upon the assimilation of spaceborne observations, Atmos. Chem. Phys., 8, 3231–3246, 2008, http://www.atmos-chem-phys.net/8/3231/2008/. 15965, 15966

Brioude, J., Cooper, O. R., Trainer, M., Ryerson, T., Holloway, J. S., Baynard, T., Peischl, J., Warneke, C., Neuman, J. A., Gouw, J. D., Stohl, A., Eckhardt, S., Frost, G. J., McKeen, S. A., Hsie, E., Fehsenfeld, F. C., and Nédélec, P.: Mixing between a stratospheric intrusion and a biomass burning plume, Atmos. Chem. Phys., 7, 4229–4235, 2007, http://www.atmos-chem-phys.net/7/4229/2007/. 15950

Cho, J., Newell, R., Browell, E., Grant, W., Butler, C., and Fenn, M.: Observation of pollution plume capping by a tropopause fold, Geophys. Res. Lett., 28, 3243–3246, 2001. 15951

Cros, B., Delmas, R., Clairac, B., LoembaNdembi, J., and Fontan, J.: Survey of ozone concentration in an equatorial region during the rainy sason, J. Geophys. Res., 92, 9772–9778, 1987. 15943

Delon, C., Reeves, C. E., Stewart, D. J., Sera, D., Dupont, R., Mari, C., Chaboureau, J., and Tulet, P.: Biogenic nitrogen oxide emissions from soils – impact on NO_x and ozone over West Africa during AMMA (African Monsoon Multidisciplinary Experiment): modelling study, Atmos. Chem. Phys., 8, 2351–2363, 2008, http://www.atmos-chem-phys.net/8/2351/2008/. 15961

Drobinski, P., Saïd, F., Ancellet, G., Arteta, J., Augustin, P., Bastin, S., Brut, A., Caccia, J., Campistron, B., Cautenet, S., Colette, A., Coll, I., Corsmeier, U., Cros, B., Dabas, A., Delbarre, H., Dufour, A., Durand, P., Guénard, V., Hasel, M., Kalthoff, N., C.Kottmeier, Lasry, F., Lemonsu, A., Lohou, F., Masson, V., Menut, L., Moppert, C., Peuch, V., Puygrenier, V., Reitebuch, O., and Vautard, R.: Regional transport and dilution during high-pollution episodes in southern France: Summary of findings from the Field Experiment to Constraint Models of Atmospheric Pollution and Emissions Transport (ESCOMPTE), J. Geophys. Res., 112, D13105, doi:10.1029/2006JD007494, 2007. 15956

Fontan, J., Druilhet, A., Benech, B., Lyra, R., and Cros, B.: The DECAFE experiments: overview and meteorology, J. Geophys. Res., 97, 6123–6136, 1992. 15943

Galy-Lacaux, C. and Modi, A. I.: Precipitation Chemistry in the Sahelian Savanna of Niger, Africa, J. Atmos. Chem., 30(3), 319–343, doi:10.1023/A:1006027730377, 1998. 15943

Heikes, B. G., Lee, M., Bradshaw, J., Sandholm, S., Davis, D. D., Crawford, J., Rodriguez, J., Liu, S., McKeen, S., Thornton, D., Bandy, A., Gregory, G., Talbot, R., and Blake, D.: Hydrogen peroxide and methylhydroperoxide distributions related to ozone and odd hydrogen over the

North Pacific in the fall of 1991, J. Geophys. Res., 101, 1891–1905, 1996. 15959
Jonquieres, I., Marenco, A., Maalej, A., and Rohrer, F.: Study of ozone formation and transatlantic transport from biomass burning emissions over West Africa during the airborne TROPospheric OZone campaigns TROPOZ I and TROPOZ II, J. Geophys. Res., 103, 19 059–19 073, 1998. 15943
Kowol-Santen, J. and Ancellet, G.: Mesoscale analysis of transport across the subtropical tropopause, Geophys. Res. Lett., 27, 3345–3348, 2000. 15955
Lazrus, A., Kok, L., Lind, J., Gitlin, S., Heikes, B., and Shetter, R.: Automated fluorometric method for hydrogen peroxide in air, Anal. Chem., 58, 594–597, 1988. 15946, 15947
Lee, M., Heikes, B., Jacob, D., Sachse, G., and Anderson, B.: Hydrogen peroxide, organic hydroperoxide, and formaldehyde as primary pollutants from biomass burning, J. Geophys. Res., 102(D1), 1301–1309, 1997. 15960
Mari, C. H., Cailley, G., Corre, L., Saunois, M., Attié, J. L., Thouret, V., and Stohl, A.: Tracing biomass burning plumes from the Southern Hemisphere during the AMMA 2006 wet season experiment, Atmos. Chem. Phys., 8, 3951–3961, 2008, http://www.atmos-chem-phys.net/8/3951/2008/. 15957
Marion, T., Perros, P., Losno, R., and Steiner, R.: Ozone Production Efficiency in Savanna and Forested Areas during the EXPRESSO Experiment, J. Atmos. Chem., 38(1), 3–30, doi:10.1023/A:1026585603100, 2001. 15948
Nédélec, P., Cammas, J., Thouret, V., Athier, G., Cousin, J., Legrand, C., Abonnel, C., Lecoeur, F., Cayez, G., and Marizy, C.: An improved infrared carbon monoxide analyser for routine measurements aboard commercial Airbus aircraft: technical validation and first scientific results of the MOZAIC III programme, Atmos. Chem. Phys., 3, 1551–1564, 2003, http://www.atmos-chem-phys.net/3/1551/2003/. 15946
Parrish, D. D., Holloway, J. S., Trainer, M., Murphy, P. C., Forbes, G. L., and Fehsenfeld, F. C.: Relationship between ozone and carbon monoxide at surface sites in the North Atlantic region, J. Geophys. Res., 103, 13 357–13 376, 1998. 15951
Sauvage, B., Thouret, V., Cammas, J. P., Gheusi, F., Athier, G., and Nedelec, P.: Tropospheric ozone over Equatorial Africa: regional aspects from the MOZAIC data, Atmos. Chem. Phys., 5, 311–335, 2005, http://www.atmos-chem-phys.net/5/311/2005/. 15957
Sauvage, B., Gheusi, F., Thouret, V., Cammas, J., Duron, J., Escobar, J., Mari, C., Mascart, P., and Pont, V.: Medium-range mid-tropospheric transport of ozone and precursors over Africa:

two numerical case studies in dry and wet seasons, Atmos. Chem. Phys., 7, 5357–5370, 2007, http://www.atmos-chem-phys.net/7/5357/2007/. 15943, 15950, 15956

Snow, J., Heikes, B., O'Sullivan, D., Shen, E., Fried, A., and Walega, J.: Hydrogen peroxide and methylhydroperoxide mixing ratios over North America and the North Atlantic during INTEX-NA., J. Geophys. Res., 112, D12S07, doi:10.1029/2006JD007746, 2007. 15959, 15960

Stewart, D. J., Taylor, C. M., Reeves, C. E., and McQuaid, J. B.: Biogenic nitrogen oxide emissions from soils: impact on NOx and ozone over west Africa during AMMA (African Monsoon Multidisciplinary Analysis): observational study, Atmos. Chem. Phys., 8, 2285–2297, 2008, http://www.atmos-chem-phys.net/8/2285/2008/. 15961

Stohl, A., Hittenberger, M., and Wotawa, G.: Validation of the Lagrangian particle dispersion model FLEXPART against large scale tracer experiment data, Atmos. Environ., 32, 4245–4264, 1998. 15953

Stohl, A., Eckhardt, S., Forster, C., James, P., Spichtinger, N., and Seibert, P.: A replacement for simple back trajectory calculations in the interpretation of atmospheric trace substance measurements, Atmos. Environ., 36, 4635–4648, 2002. 15953

Zhang, J., Rao, S., and Daggupaty, S.: Meteorological processes and ozone exceedances in the Northeastern United States during the 12-16 July 1995 episode, J. Appl. Meteorol., 37, 776–789, 1998. 15956

Table 1. Classification of the air masses.

Date	13 August 12:13–15:21 UT	19 August a.m. 9:14–12:08 UT	19 August p.m. 13:42–16:27 UT	20 August 14:03–17:30 UT
Type I air mass	CO>130 O_3<50 RH>50% 11.5 km, 6°–11° N 8 km, 6° N	CO>160 O_3<50 RH>50%, NO_x<0.1 10 km, 2°–3° N		
Type II air mass		CO<110 O_3>70 RH<30% NO_x<0.3 10 km 11°–14° N	CO<110 O_3>70 RH<30% NO_x<0.5 7–10 km 11°–14° N	CO<110 O_3>70 RH<30% NO_x<0.5 7.5 km 11.5°–14° N
Type III air mass		CO>200 NO_x>1 <4 km 6° N	CO>200 NO_x>1 <4 km 6° N	
Type IV air mass		CO≈150 O_3≈70 RH<30% NO_x<0.3 7.5 km 2°–4° N		
Type V air mass		CO≈130 O_3≈60 RH>50% NO_x≈0.5 7.5 km 4°–6° N	CO≈110 O_3≈60 RH≈80% NO_x>0.7 7.5 km 8°–10° N	CO<110 O_3≈55 RH>40% NO_x>0.7 5.5 km 11°–13° N

ACPD
8, 15941–15996, 2008

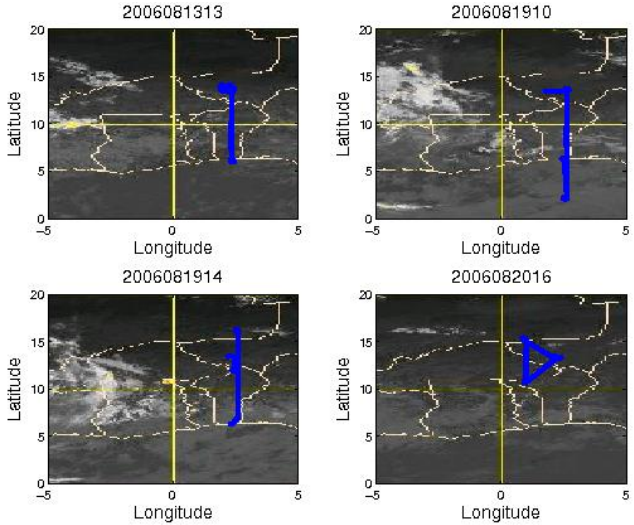

Fig. 1. Aircraft tracks superimposed on MSG/Meteosat pictures at flight mid-time.

ACPD
8, 15941–15996, 2008

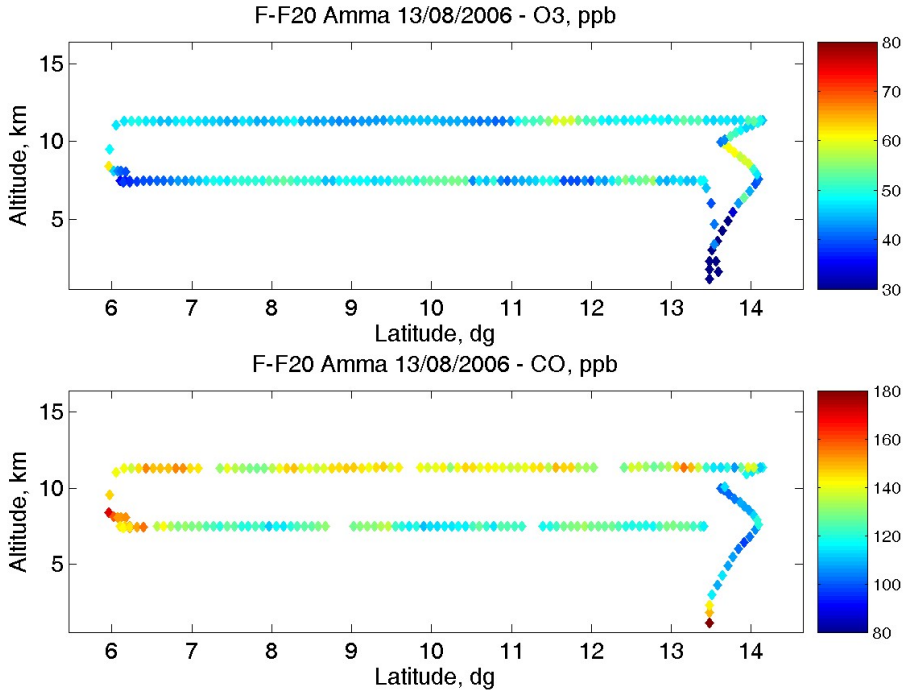

Fig. 2a. Altitude vs. latitude distribution of O_3 and CO mixing ratio in ppb along the 13 August LRT flight (no NO_x measurements).

ACPD
8, 15941–15996, 2008

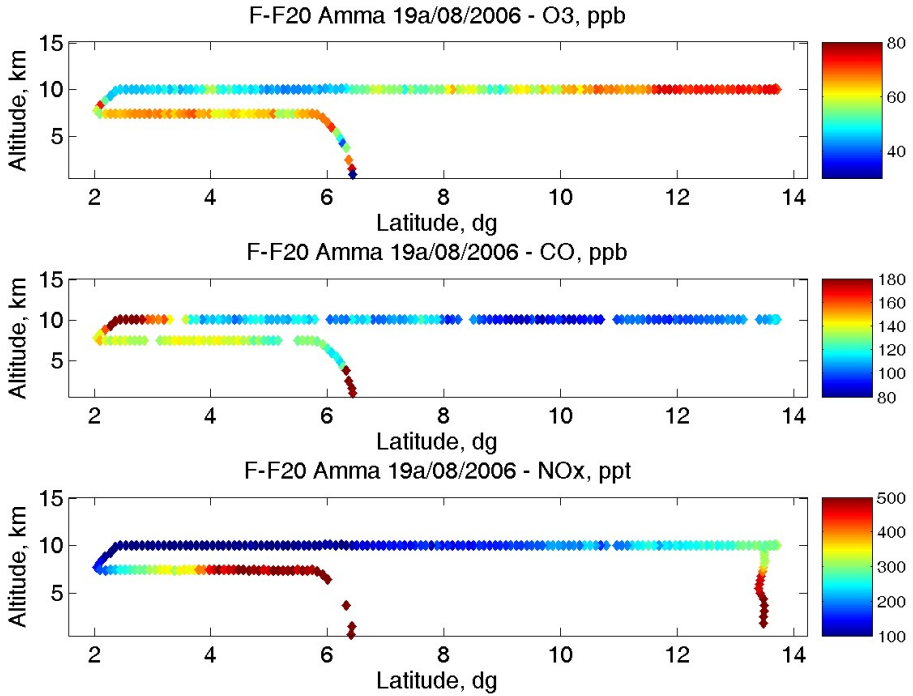

Fig. 2b. Altitude vs. latitude distribution of O_3, CO, and NO_x mixing ratio in ppb along the 19 August LRT flight (a.m.).

ACPD
8, 15941–15996, 2008

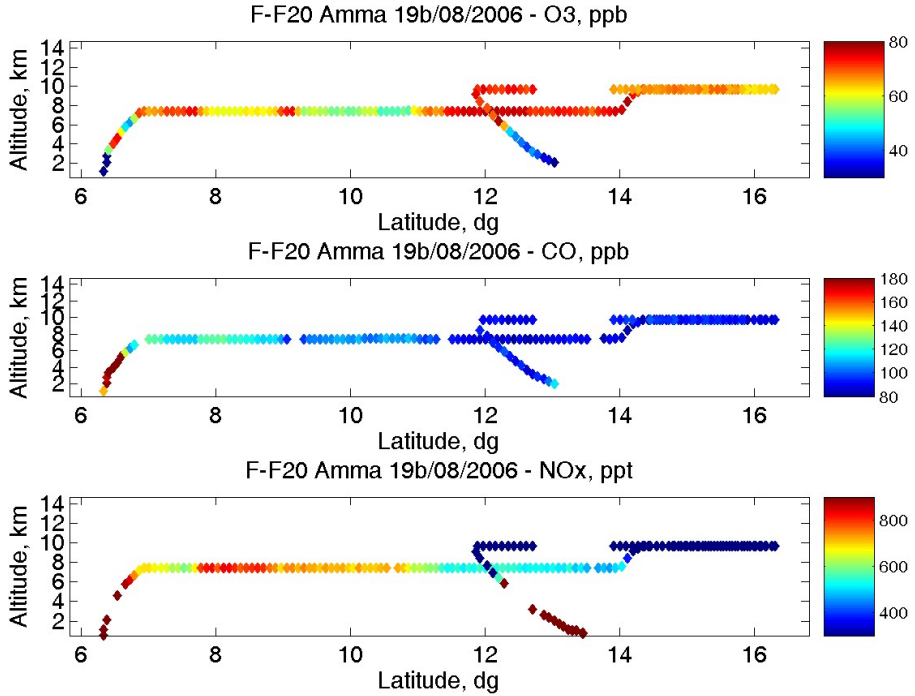

Fig. 2c. Altitude vs. latitude distribution of O_3, CO, and NO_x mixing ratio in ppb along the 19 August LRT flight (p.m.).

ACPD

8, 15941–15996, 2008

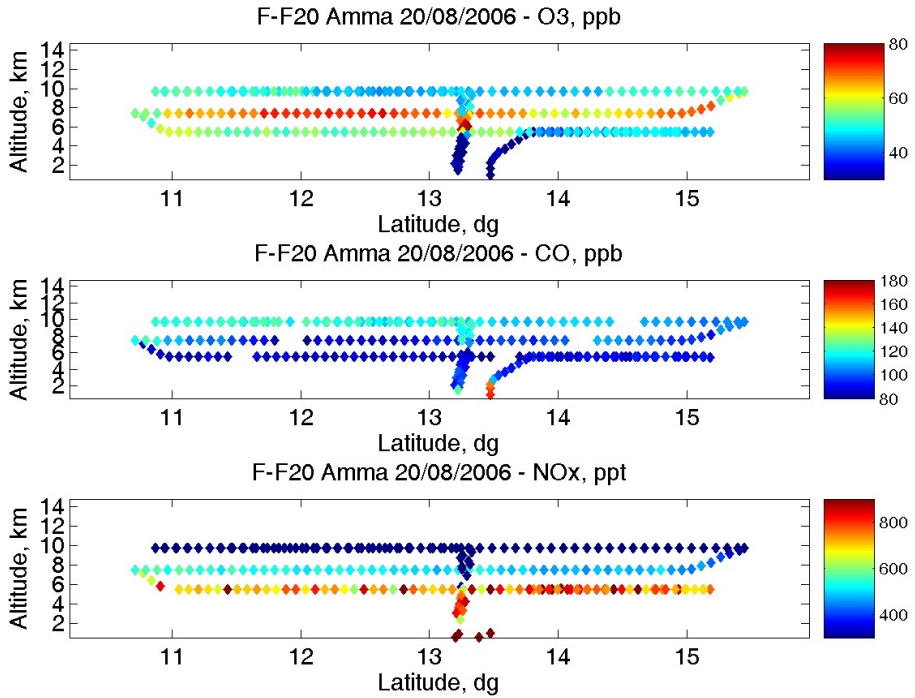

Fig. 2d. Altitude vs. latitude distribution of O_3, CO, and NO_x mixing ratio in ppb along the 20 August LRT flight.

ACPD
8, 15941–15996, 2008

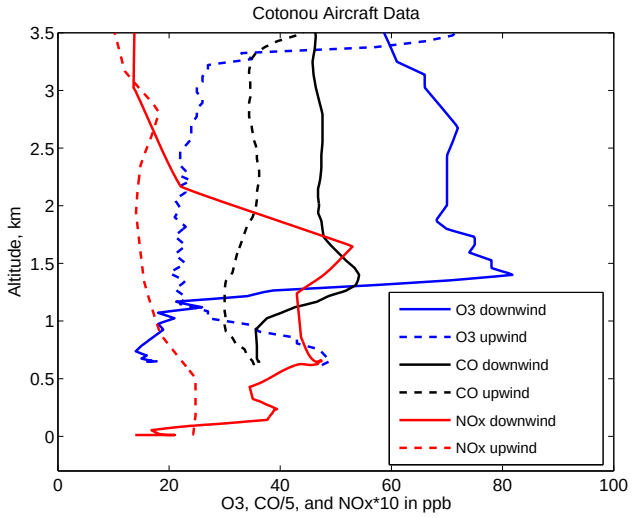

Fig. 3. Profiles of O_3, CO and NO_x in ppb during landing (19 August a.m. – downwind) and take-off (19 August p.m. – upwind) from Cotonou (Benin).

ACPD
8, 15941–15996, 2008

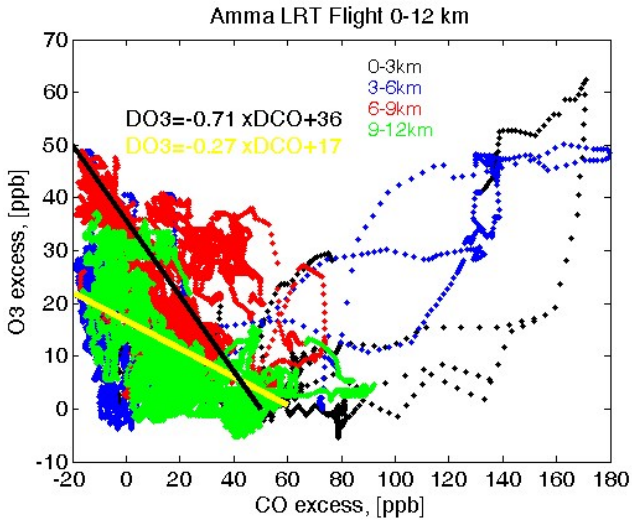

Fig. 4. Scatter plot of O3 excess vs. CO excess in ppb as measured by the F-F20 during the four LRT flights.

ACPD
8, 15941–15996, 2008

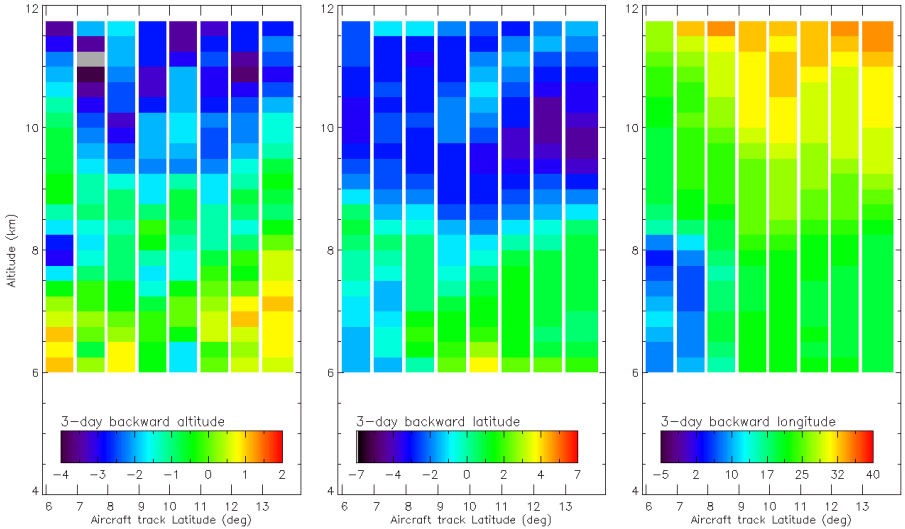

Fig. 5a. Altitude vs. latitude FLEXPART plots of particles released along the 13 August flight track. The color scale indicates the altitude (left in km), latitude (middle in °), and longitude (right in °) change of the air mass between the observation time and its position three days before.

ACPD
8, 15941–15996, 2008

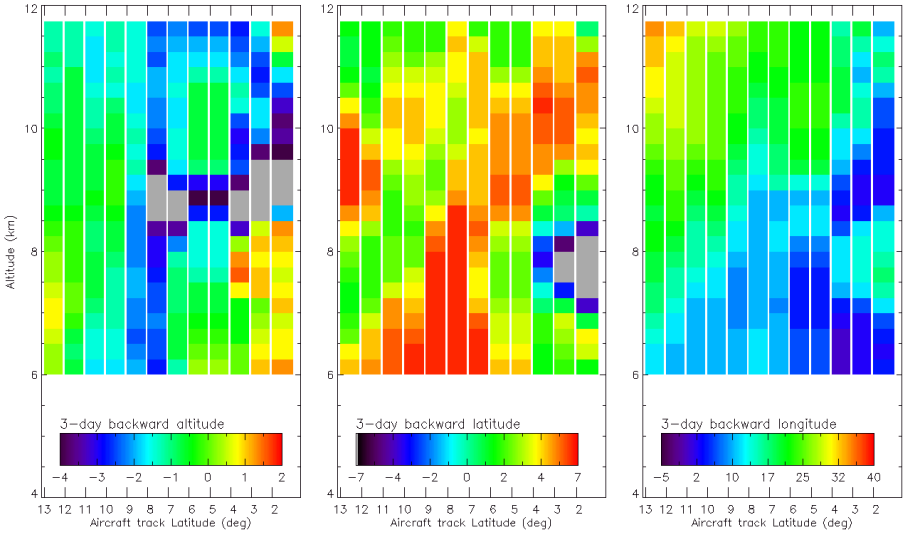

Fig. 5b. Altitude vs. latitude FLEXPART plots of particles released along the 19 August a.m. flight track. The color scale indicates the altitude (left in km), latitude (middle in °), and longitude (right in °) change of the air mass between the observation time and its position three days before.

ACPD
8, 15941–15996, 2008

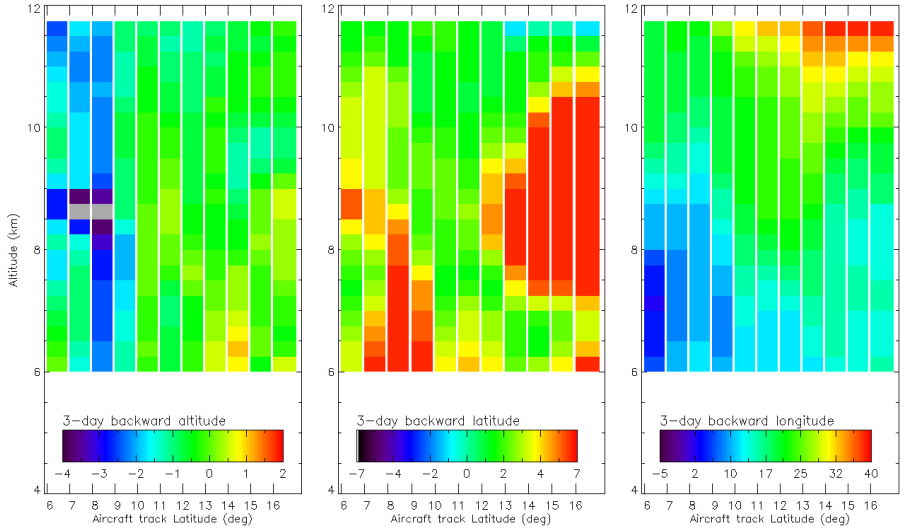

Fig. 5c. Altitude vs. latitude FLEXPART plots of particles released along the 19 August p.m. flight track. The color scale indicates the altitude (left in km), latitude (middle in °), and longitude (right in °) change of the air mass between the observation time and its position three days before.

ACPD
8, 15941–15996, 2008

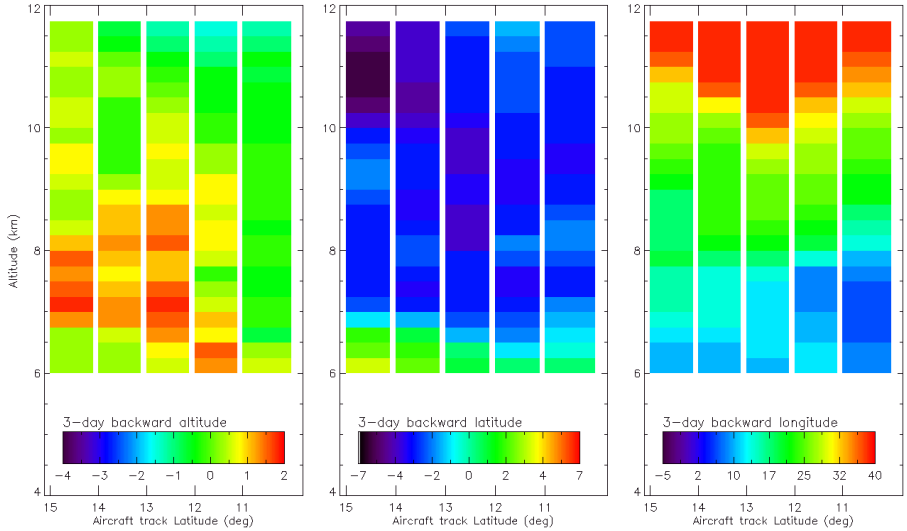

Fig. 5d. Altitude vs. latitude FLEXPART plots of particles released along the 20 August flight track. The color scale indicates the altitude (left in km), latitude (middle in °), and longitude (right in °) change of the air mass between the observation time and its position three days before.

ACPD
8, 15941–15996, 2008

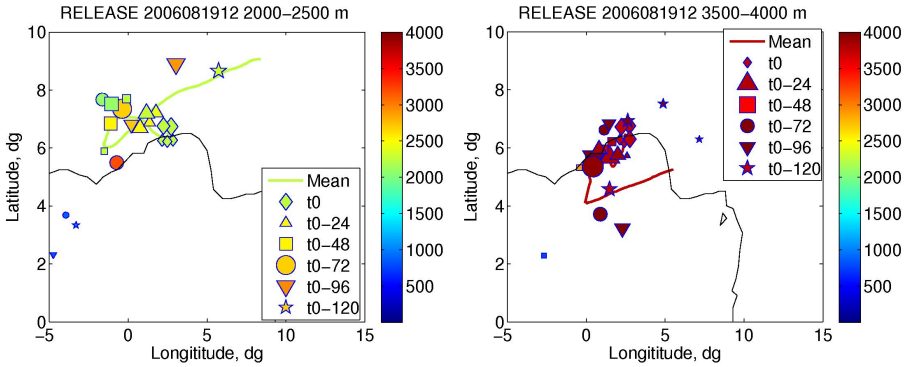

Fig. 6. 5-days FLEXPART backward time position of five clusters of the 2000 particles released between 2 and 2.5 km (left panel) and between 3.5 and 4 km (right panel) over Cotonou on 19 August at 12:00 UT. The clusters are plotted every 24 h, the color corresponds to their altitude, and the size of each cluster is proportional to the number of particles.

ACPD
8, 15941–15996, 2008

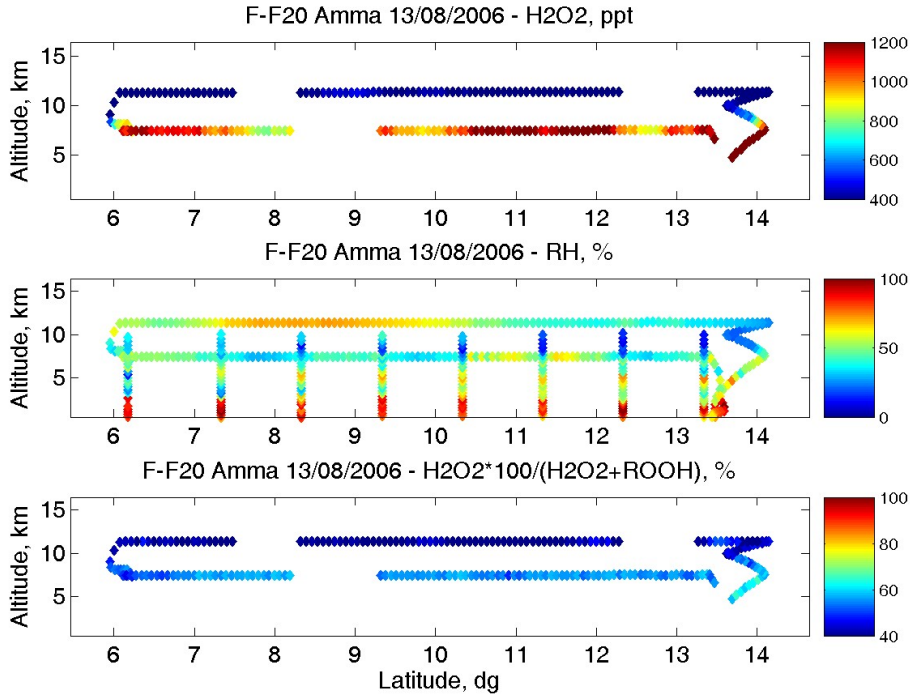

Fig. 7a. Altitude vs. latitude distribution of H_2O_2 mixing ratio in ppt, relative humidity in % and fraction of H_2O_2 over total organic peroxides in % along the 13 August flight.

ACPD
8, 15941–15996, 2008

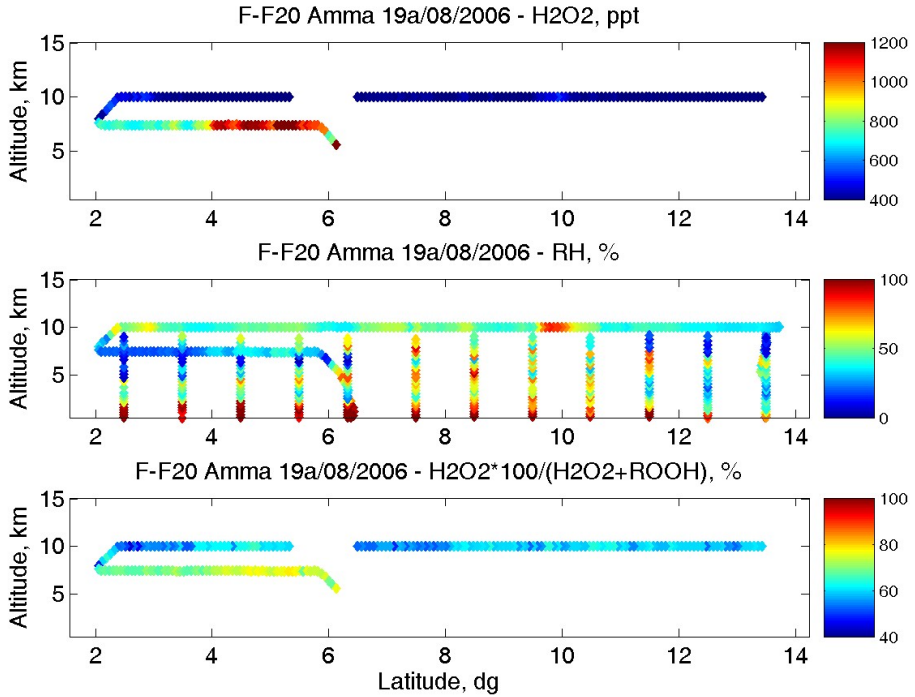

Fig. 7b. Altitude vs. latitude distribution of H_2O_2 mixing ratio in ppt, relative humidity in % and fraction of H_2O_2 over total organic peroxides in % along the 19 August a.m. flight.

ACPD
8, 15941–15996, 2008

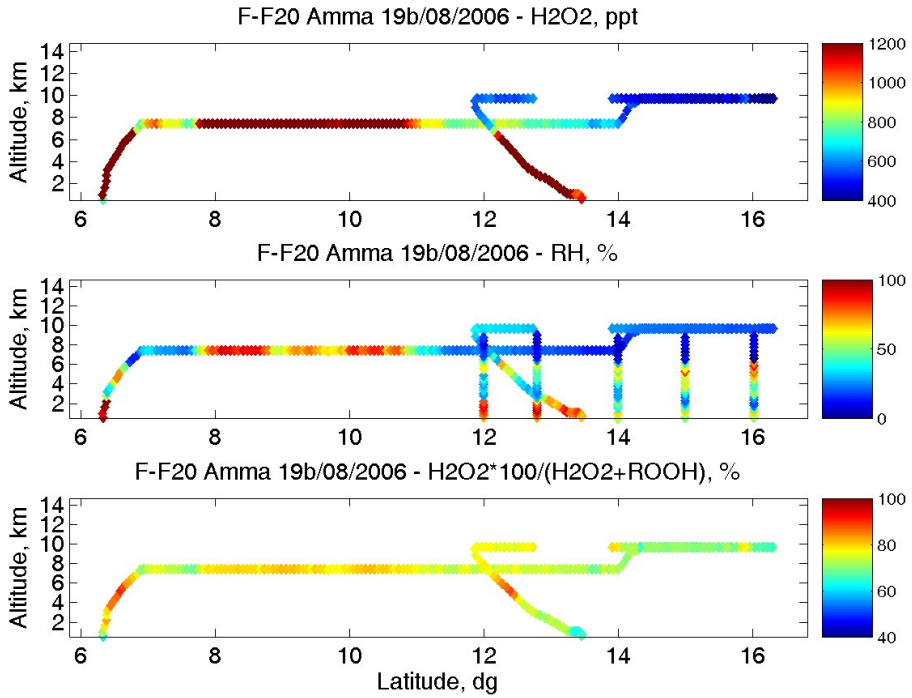

Fig. 7c. Altitude vs. latitude distribution of H_2O_2 mixing ratio in ppt, relative humidity in % and fraction of H_2O_2 over total organic peroxides in % along the 19 August p.m. flight.

ACPD
8, 15941–15996, 2008

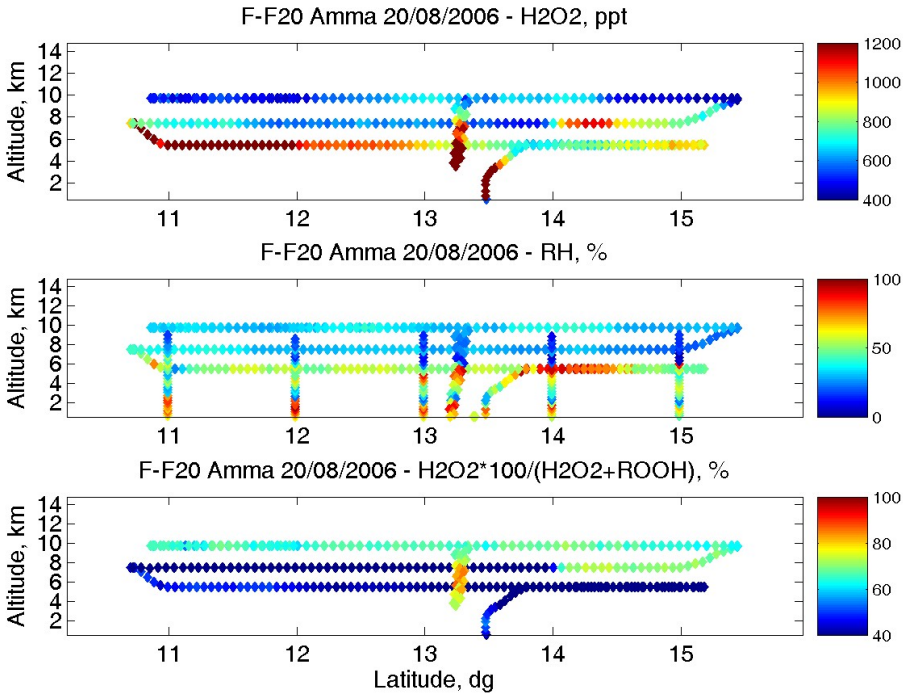

Fig. 7d. Altitude vs. latitude distribution of H_2O_2 mixing ratio in ppt, relative humidity in % and fraction of H_2O_2 over total organic peroxides in % along the 20 August flight.

ACPD
8, 15941–15996, 2008

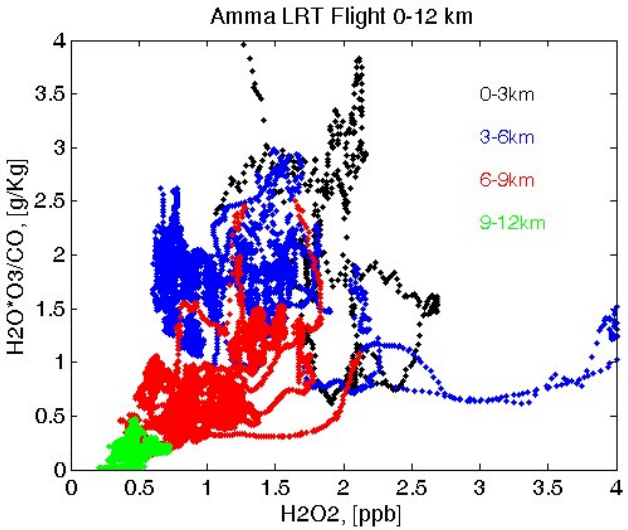

Fig. 8. Scatter plot of $[H_2O]^*[O_3]/[CO]$ in g/kg vs. H_2O_2 in ppt as measured by the F-F20 during for the four LRT flights. The measurements are colored with altitude (4 classes with a 3-km thickness within the range to 0–12 km).

ACPD
8, 15941–15996, 2008

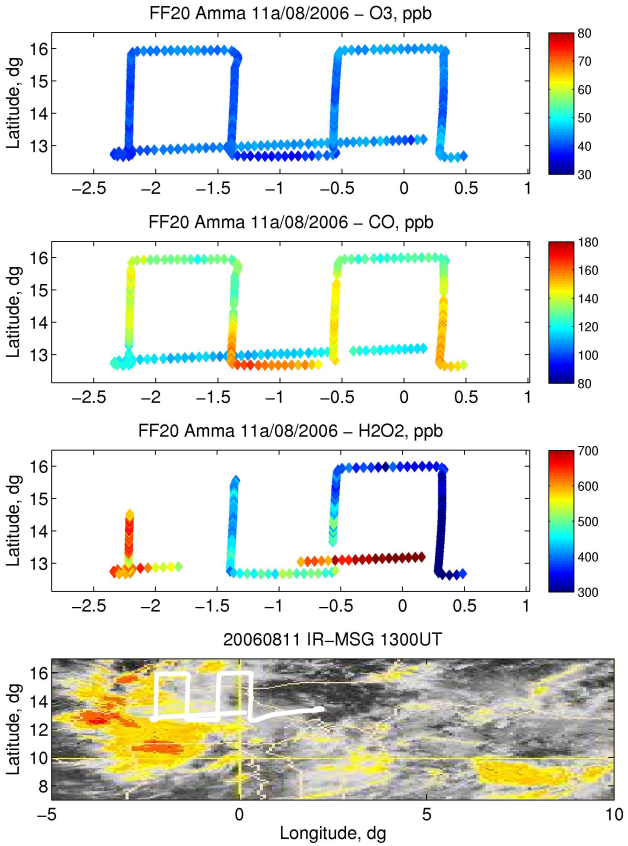

Fig. 9. Latitude vs. longitude distribution of O_3, CO in ppb, and H_2O_2 in ppt along the 11 August MCS flight. The track has been superimposed on the MSG/Meteosat picture taken at the beginning of the flight.

ACPD
8, 15941–15996, 2008

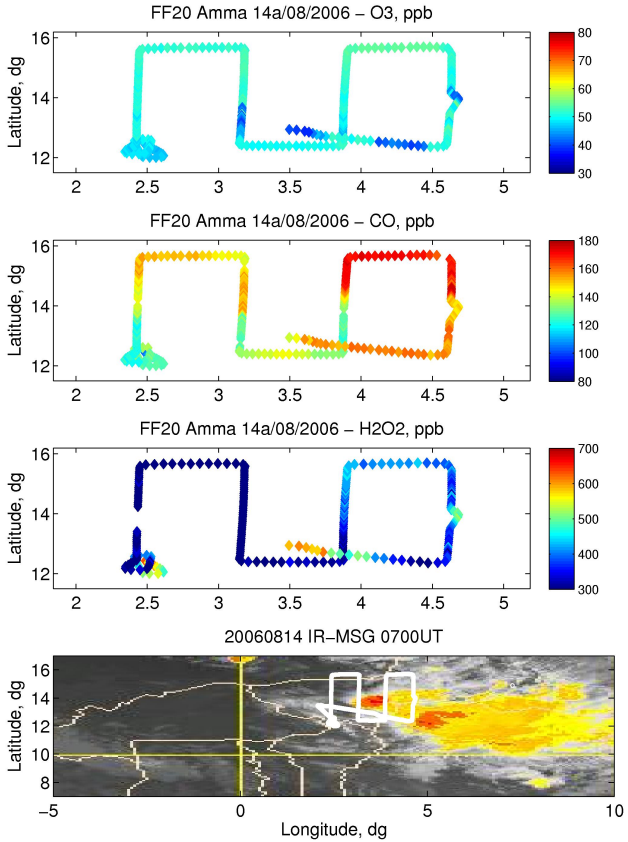

Fig. 10. Latitude vs. longitude distribution of O_3, CO in ppb, and H_2O_2 in ppt along the 14 August MCS flight. The track has been superimposed on the MSG/Meteosat picture taken at the beginning of the flight.

ACPD
8, 15941–15996, 2008

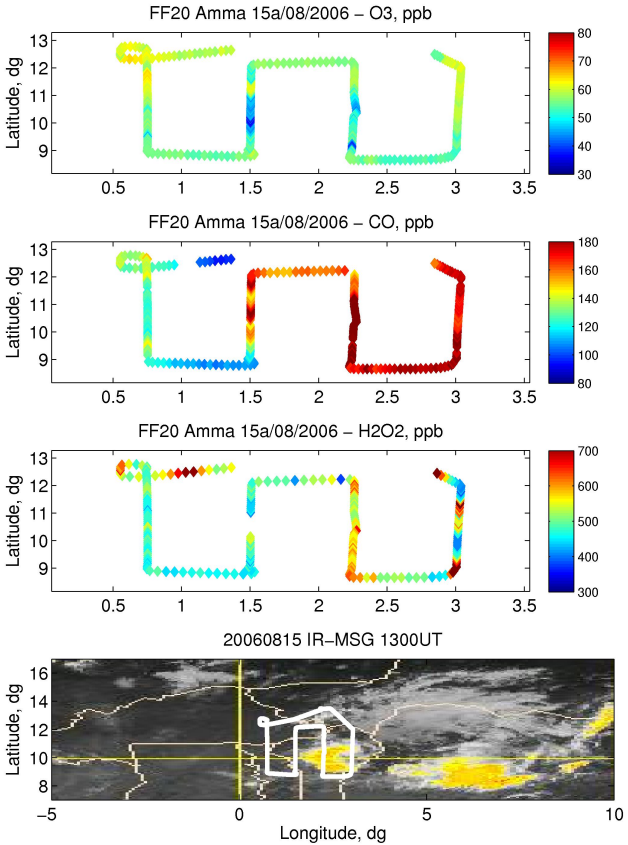

Fig. 11. Latitude vs. longitude distribution of O_3, CO in ppb, and H_2O_2 in ppt along the 15 August MCS flight. The track has been superimposed on the MSG/Meteosat picture taken at the beginning of the flight.

ACPD
8, 15941–15996, 2008

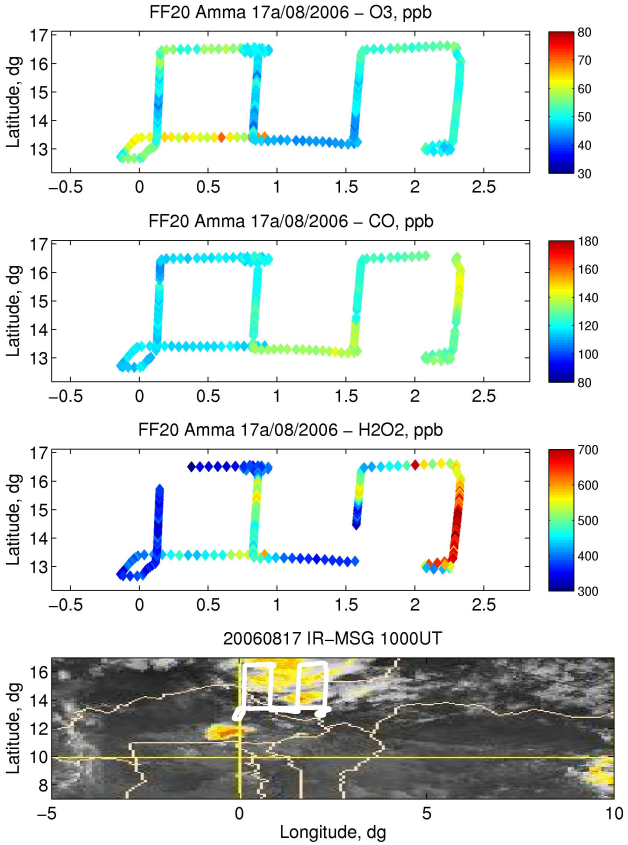

Fig. 12. Latitude vs. longitude distribution of O_3, CO in ppb, and H_2O_2 in ppt along the 17 August MCS flight. The track has been superimposed on the MSG/Meteosat picture taken at the beginning of the flight.

ACPD
8, 15941–15996, 2008

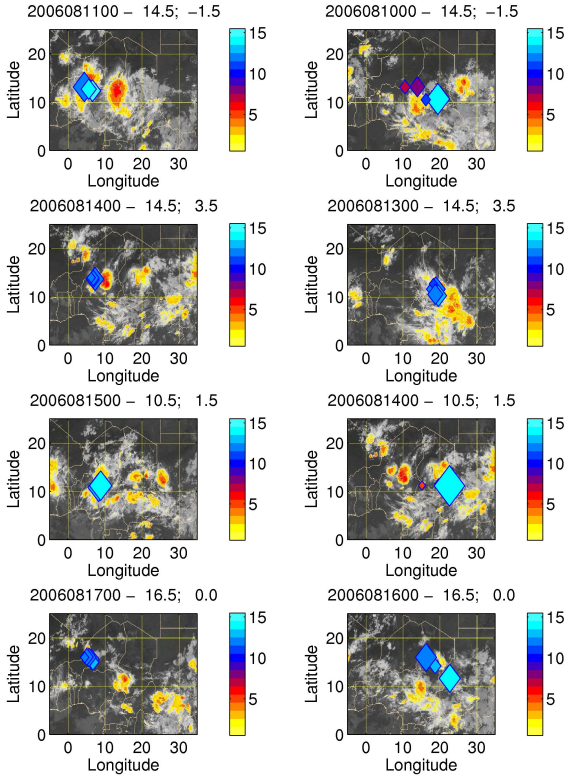

Fig. 13. Plot on MSG/meteosat pictures of the five FLEXPART clusters released at the center of the upper altitude flight track survey around the MCS studied on 11 August, 14 August, 15 August and 17 August (top to bottom). Cluster position and altitude (color code) are given at 00:00 UT on the measurement day (left) and 00:00 UT on the previous day (right). The size of each cluster is proportional to the number of particles.

ACPD
8, 15941–15996, 2008

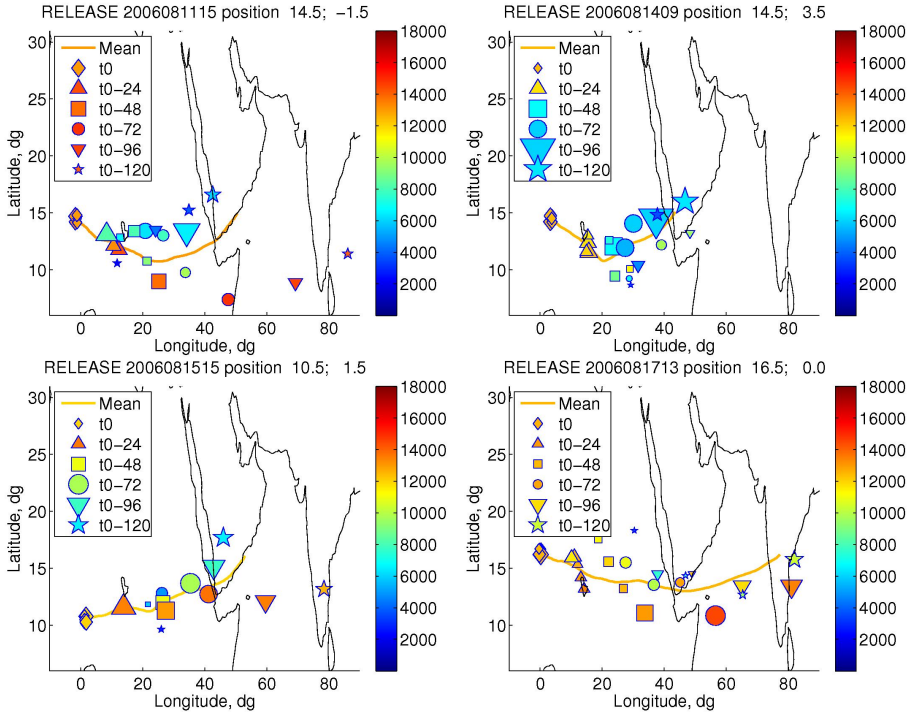

Fig. 14. 5-days FLEXPART backward time position of five clusters of the 2000 particles released at the center of the upper altitude flight track survey around the MCS studied on 11 August (upper left), 14 August (upper right), 15 August (lower left) and 17 August (lower right). The clusters are plotted every 24 h, the color corresponds to their altitude, and the size of each cluster is proportional to the number of particles.

ACPD
8, 15941–15996, 2008

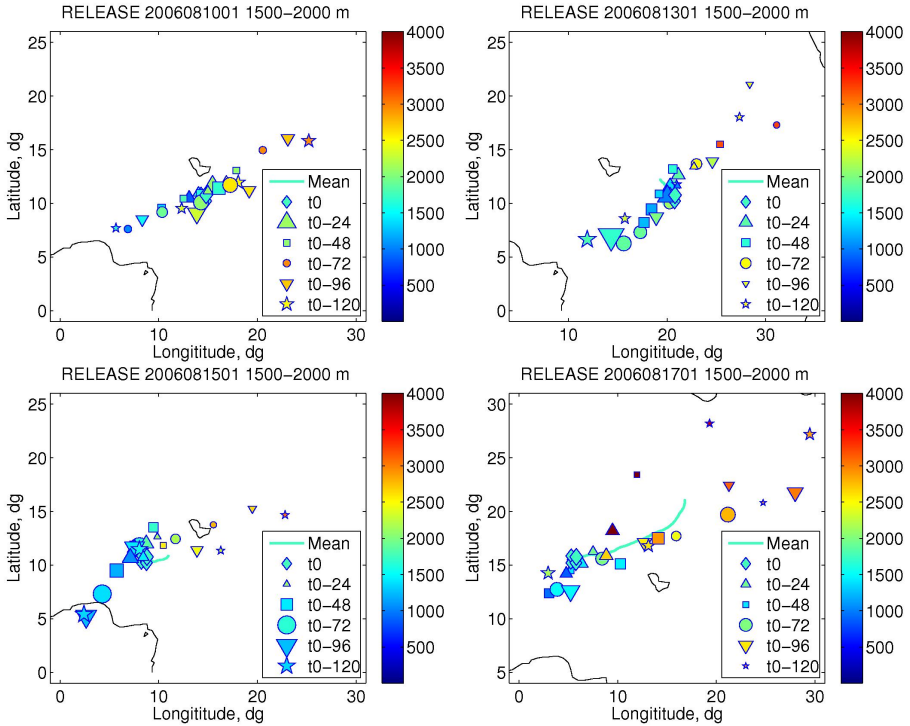

Fig. 15. 5-days FLEXPART backward time position of five clusters of the 2000 particles released at low altitudes (1500–200 m) below a MCS position at 00:00 UT on 10 August (upper left), 13 August (upper right), 15 August (lower left) and 17 August (lower right). The 10 August and 13 August MCS have developed along the trajectories shown in Fig. 14, while the 15 August, 17 August MCS are the studied MCS. The clusters are plotted every 24 h, the color corresponds to their altitude, and the size of each cluster is proportional to the number of particles.

ACPD
8, 15941–15996, 2008